ACS APPLIED MATERIALS & INTERFACES

Research Article

www.acsami.org

# High-Pressure Solvent Vapor Annealing with a Benign Solvent To Rapidly Enhance the Performance of Organic Photovoltaics

Buyoung Jung, Kangmin Kim, Yoomin Eom, and Woochul Kim*

School of Mechanical Engineering, Yonsei University, Seoul 120-749, South Korea

Supporting Information

**ABSTRACT:** A high-pressure solvent vapor annealing (HPSVA) treatment is suggested as an annealing process to rapidly achieve high-performance organic photovoltaics (OPVs); this process can be compatible with roll-to-roll processing methods and uses a benign solvent: acetone. Solvent vapor annealing can produce an advantageous vertical distribution in the active layer; however, conventional solvent vapor annealing is also time-consuming. To shorten the annealing time, high-pressure solvent vapor is exposed on the active layer of OPVs. Acetone is a nonsolvent for poly(3-hexylthiophene-2,5-diyl) (P3HT), but it can dissolve small amounts of 1-(3-methoxycarbonyl)-propyl-1,1-phenyl-(6,6)$C_{61}$ (PCBM). Acetone vapor molecules can penetrate into the active layer under high vapor pressure conditions to alter the morphology. HPSVA induces a PCBM-rich phase near the cathode and facilitates the transport of free charge carriers to the electrode. Although P3HT is not soluble in acetone, locally rearranged P3HT crystallites are generated. The performance of OPV films was enhanced after HPSVA; the film treated at 30 kPa for 10 s showed optimum performance. Additionally, this HPSVA method could be adapted for mass production because the temporary exposure of films to high-pressure acetone vapor in ambient conditions also improved performance.

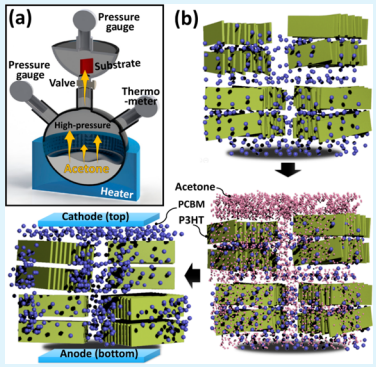


**KEYWORDS:** *organic photovoltaics, solvent vapor annealing, morphology generation, vertical segregation, mass production*

## 1. INTRODUCTION

The fabrication of organic photovoltaics (OPVs) has attracted a great deal of attention in the past decade due to the advantages of lightweight, flexibility, solution processability, and relatively low cost. To enhance the power conversion efficiency (PCE) of OPVs, the morphology of the active layer must be properly composed. The crystallized polymer domain size, fullerene aggregate size, and polymer−fullerene intercalated zones should be balanced. In addition, appropriate distribution of hole- and electron-conducting materials in the vertical direction between the two electrodes is required. In order to facilitate charge transport toward each electrode, hole-conducting materials (polymer) should be placed near the anode, whereas the electron-conducting materials (fullerene derivatives) should be placed near the cathode.[1−5]

To achieve this desirable distribution, precise control of the morphology is critical. The morphology of the active layer can be altered through post-treatment methods such as thermal,[6−10] solvent vapor,[6,7,11−14] microwave,[15−17] and microwave-assisted solvent vapor annealing,[18] as well as solvent soaking[18−20] and additive insertion.[21−25] The conventional post-treatment method, i.e., prethermal annealing (Pre-TA; TA before metal deposition), yields an undesirable vertical distribution where the polymer-rich phase is often near the cathode. This undesirable distribution is caused by the surface energy of the polymer material, which is lower than that of the fullerene-derivative material. Representative hole- and electron-conducting materials, such as poly(3-hexylthiophene-2,5-diyl) (P3HT) and 1-(3-methoxycarbonyl)-propyl-1,1-phenyl-(6,6)$C_{61}$ (PCBM), have surface energies of 27 and 38 mN/m, respectively.[26] To reduce the total surface energy, the lower surface energy material (P3HT) needs to be closer the top surface. Alternatively, solvent vapor annealing (SVA) is an effective method to achieve the desired vertical distribution of hole- and electron-conducting materials. Various SVA methods are summarized in Table 1. When the active layer of an OPV is exposed to solvent vapor conditions, solvent molecules diffuse into the active layer and modify the morphology at the nanoscale level. Ruderer et al.[27] reported the morphology alteration in vertical and lateral direction of P3HT:PCBM film according to the various solvent such as chloroform, toluene, chlorobenzene (CB), and xylene. In the vertical direction, P3HT rich phases were detected for toluene- and CB-made films and PCBM rich phases were found for the films made using toluene and xylene. Guo et al.[28] reported the influence of chlorobenzene, 1,2-dichlorobenzene, and 1,2,4-trichlorobenzene solvents and solvent additive (1,8-diiodooctane) on the morphology of polymer film. For films made from chlorobenzene, the smallest polymer domains were obtained, due to the high volatility of the solvent. Meier et al.[29] showed that the amount of the residual solvent depends on the interaction of the polymer and thus influences on the

Received: February 23, 2015
Accepted: May 21, 2015
Published: June 10, 2015





DOI: 10.1021/acsami.5b01658
ACS Appl. Mater. Interfaces 2015, 7, 13342−13349

**Table 1. Summary of the Photovoltaic Properties of OPV Devices (P3HT:PCBM) Treated by Various Solvent Vapor Annealing Methods[a]**

| ref. | solvent | time | PCE [%] | $V_{oc}$ [V] | $J_{sc}$ [mA/cm$^2$] | FF [%] | condition |
|---|---|---|---|---|---|---|---|
| this work | acetone | 10 s | 2.09 | 0.62 | 5.6 | 60 | pressurized SVA (over SVP) |
| 28 | chlorobenzene | 5 s | 1.52 | 0.56 | 7.45 | 36 | SVA using an $N_2$ flux bubble (unknown pressure) |
| | toluene | 5 s | 1.55 | 0.56 | 6.81 | 41 | |
| | 1,2,3,4-tetrahydronaphthalene | 5 s | 0.76 | 0.6 | 3.71 | 34 | |
| 30 | tetrahydrofuran + carbon bisulfide | 5 s + 15 s | 3.9 | 0.58 | 11.01 | 61 | SVA by sequential exposure to two different solvents (below SVP) |
| 23 | acetone | 60 m | 3.29 | 0.57 | 10.72 | 54 | SVA in a covered Petri dish (at SVP) |
| | methylene chloride | | 3.27 | 0.52 | 11.44 | 55 | |
| | chloroform | | 2.66 | 0.59 | 8.22 | 55 | |
| | chlorobenzene | | 2.88 | 0.64 | 8.35 | 54 | |
| | 1,2-dichlorobenzene | | 2.86 | 0.63 | 7.76 | 59 | |
| 29 | 2-chlorophenol | 30 m | 2.1 | 0.58 | 6.89 | 52 | SVA in a vertical tube (at SVP) |

[a]SVP, solvent vapor pressure.

performance of the polymer electronic devices. Campoy-Quiles et al.[12] reported that the fullerene-derivative ratio near the top surface (in contact with the cathode) was increased after 30 min of SVA with chlorobenzene. Jo et al.[30] also demonstrated that higher concentrations of the fullerene-derivate were formed near the top surface; in their study, SVA was achieved with dichlorobenzene and optimum device performance was obtained after 2 h of exposure. There are several parameters that affect morphological changes during SVA, such as exposure time, vapor pressure, and the solubility of the active materials in the solvent. To shorten the exposure time, Burgues-Ceballos et al.[31] bubbled nitrogen gas at an ambient temperature to deliver chlorobenzene solvent vapor onto the active layer. Their exposure time was about 5 s, but the device performance did not surpass the performance of the thermally annealed devices due to a low fill factor. Under a short exposure time, disordered polymers remained, contributing to poor charge transport. Hu et al.[32] compared the performances of solvent vapor annealed OPVs using different solvents with different P3HT and PCBM solubilities. They revealed that 2-chlorophenol, which has high PCBM solubility, enhanced the performance. This improvement was caused by the fact that SVA induced PCBM to segregate toward the air surface. Tang et al.[33] applied a two-step, controlled SVA method using tetrahydrofuran and carbon disulfide. They conducted their SVA process at conditions below the solvent vapor pressure (SVP) and provided different pressure conditions by placing their substrates in different positions along a long glass tube containing the liquid solvent. The pressure was higher near the solvent surface and lower along the glass tube. Therefore, their pressure conditions were not higher than the SVP; thus, it is worthwhile to investigate the morphological effects over the SVP.

SVA is an effective method of achieving higher PCE because it allows the active layer morphology to be controlled precisely. However, this method requires relatively long processing times and/or utilizes complicated processing steps. Additionally, it normally requires the usage of toxic solvents such as chlorobenzene, dichlorobenzene, 2-chlorophenol, or carbon disulfide. These shortcomings hinder the mass production of OPVs made via SVA. Here, we suggest a novel SVA method to shorten the processing time to around 10 s. We also use a relatively benign solvent: acetone. Conventional SVA (CVSVA) methods have been conducted under the saturated vapor pressure (e.g., 1.17 kPa for chlorobenzene). In this paper, CVSVA was conducted using acetone. One hour before conducting CVSVA, 1 mL of acetone was placed in the sealed glass dish to create a saturated vapor pressure condition and the films were placed in the glass dish for several minutes. The high-pressure solvent vapor annealing (HPSVA) was conducted at pressures between 10 and 40 kPa. To create these high-pressure conditions, high-pressure acetone vapor was generated by heating acetone in a sealed 1 L flask, as shown in Figure 1a.

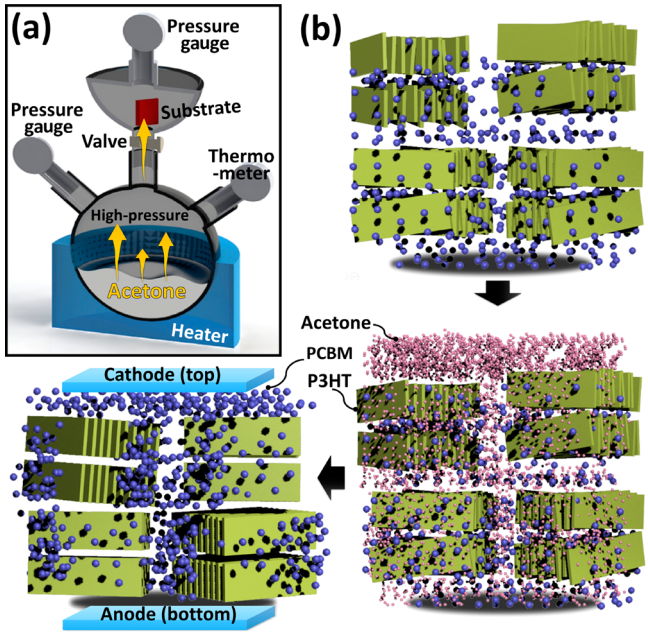


**Figure 1.** (a) Schematics of the experimental setup. The high-pressure solvent vapor is generated in the large, heated flask and transferred into the small flask through the intercept valve. (b) Schematic of HPSVA. The high-pressure acetone molecules penetrate into the active layer and selectively dissolve PCBM. This leads to a PCBM-rich phase near the top surface and closely packed P3HT crystallites.

Acetone solvent vapor molecules were evaporated in the flask once it was wrapped with a heating mantle. Above the acetone boiling point (56 °C), the pressure in the large flask increased. After reaching the target pressure, the intercept valve was opened and high-pressure solvent vapor molecules were transferred into a connected 50 mL flask. The pressure was also measured with a pressure gauge attached to the small flask,


DOI: 10.1021/acsami.5b01658
ACS Appl. Mater. Interfaces 2015, 7, 13342−13349

and it was determined that the pressure difference caused by opening the valve was less than 10%. A film in the smaller flask was annealed with high-pressure solvent vapor for a specific exposure time.

Acetone vapor has a crucial role in HPSVA. Acetone is a known nonsolvent for P3HT, but it does dissolve small amounts of PCBM.[14] The solubility of P3HT and PCBM in acetone was measured to be $10^{-3}$ and 0.15 mg/mL, respectively, via UV−vis spectroscopy. Under high-pressure conditions, many acetone molecules with high kinetic energy permeate into the active layer and selectively dissolve PCBM molecules, as shown in Figure 1b. In this process, the PCBM concentration in acetone varies in the vertical direction, causing PCBM molecules to diffuse toward the surface. Acetone molecules do not directly affect P3HT because acetone is a nonsolvent for P3HT. However, disordered P3HT lamellae are locally rearranged during HPSVA. After HPSVA, the volatile acetone molecules immediately evaporate (due to their low boiling point of 56 °C), thereby maintaining the desired vertical distribution of the active layer.

The HPSVA film showed increased $J_{sc}$ because of the large interfacial area between P3HT and PCBM and the advantageous vertical distribution. The local arrangement of the P3HT lamellae increased the interfacial area and facilitated exciton dissociation. Also, the PCBM-rich phase near the cathode facilitated charge extraction near the electrode. The HPSVA film also exhibited reduced FF because of its small phase separation. On the basis of multiplication of the increased $J_{sc}$ and decreased FF, the overall PCE of the HPSVA film was found to be similar or higher than that of the Pre-TA film.

## 2. RESULTS AND DISCUSSION

Time-of-flight secondary ion mass spectrometry (TOF-SIMS) measurements were conducted to investigate the vertical distribution of the hole- and electron-conducting materials in the active layer. Although carbon atoms exist in both P3HT and PCBM, sulfur atoms exist only in P3HT. Thus, the ratio of sulfur to carbon atoms provides information about the P3HT component ratio in the P3HT/PCBM bulk-heterojunction. In Figure 2, untreated and thermally annealed films show a high sulfur/carbon ratio near the top surface, which indicates the presence of a P3HT-rich phase. The distribution of P3HT (which has lower surface energy than PCBM) near the top surface stabilizes the surface energy.[15,26] However, this vertical distribution hinders electron transfer to the cathode. Conversely, high-pressure solvent vapor annealed films commonly exhibit a low P3HT ratio near the top surface, as shown in Figure 2. This implies that a relatively large PCBM component exists near the top surface, which could facilitate electron transport to the cathode.

The thicknesses of films annealed at excessively higher pressure (40 kPa) or for quite a longer exposure time (300 s) were decreased to 70 or 90 nm, respectively, as shown in Figure 2. Closely packed acetone molecules surrounding the films exert pressure on the active layer and could lead to a closely packed P3HT and PCBM bulk heterojunction. The thinner active layer facilitates free charge transfer to each electrode due to the decreased distance that a hole/electron has to travel. However, the decreased active layer is unfavorable to light absorption.

To observe the characteristics of P3HT crystallites, X-ray diffraction (XRD) measurements were taken, as shown in Figure 3. Crystallized P3HT molecules have a lamellar structure

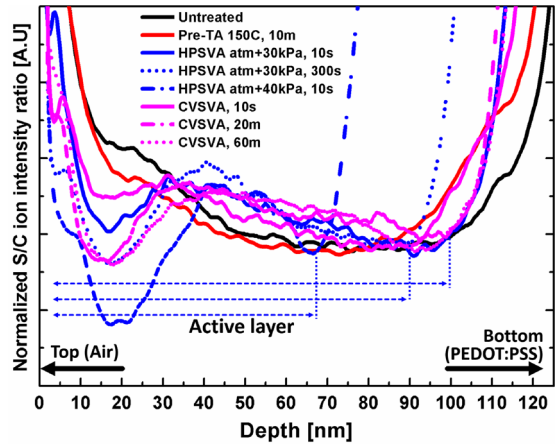


**Figure 2.** Secondary ion mass spectroscopy (SIMS) profiles of untreated, prethermally annealed (Pre-TA), conventional solvent vapor annealed (CVSVA), and high-pressure solvent vapor annealed (HPSVA) films with vapor pressure and execution time. The lines represent the ratio of sulfur counts (in P3HT) to carbon counts (in both P3HT and PCBM), indicating the amount of P3HT in the bulk-blend.

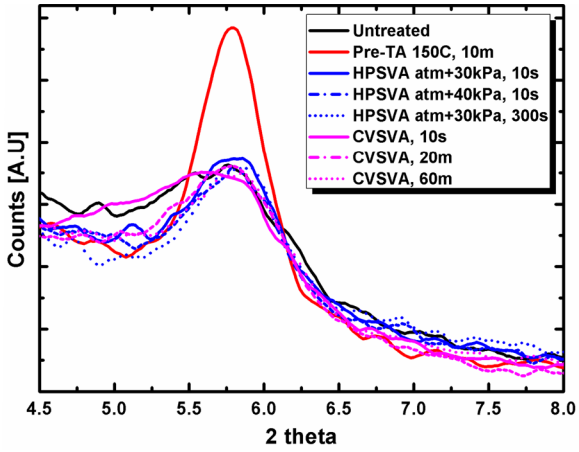


**Figure 3.** X-ray diffraction (XRD) profiles of untreated, prethermally annealed (Pre-TA), conventional solvent vapor annealed (CVSVA), and high-pressure solvent vapor annealed (HPSVA) films with vapor pressure and execution time.

with an alkane side chain spacing of about 16 Å and a $\pi-\pi$ stacked conjugated backbone spacing of 3.8 Å.[34−36] The edge-on peak, corresponding to the alkane side chain stacked in the lamellar structure, is observed to be near 5.8° ($2\theta$) (see Figure 3). The peak intensities of HPSVA films are weak compared to those of thermally annealed films and are rather analogous to those of untreated films. This means that additional lamellar structures are not formed during HPSVA. As mentioned above, acetone is a nonsolvent for P3HT, so P3HT has little chance of dissolving fully and crystallizing. However, the average full width at half-maximum (fwhm) value of the HPSVA films is ~0.64°, which is narrower than that of the untreated film (0.86°). A broader fwhm is observed when crystallites are not uniform; the narrower FWHMs of the HPSVA films indicate that disordered P3HT lamellae are rearranged during HPSVA. Although P3HT is not soluble in acetone, temporary vacancies may be generated during the process of PCBM diffusion, allowing P3HT lamellae to be locally rearranged.[37]


DOI: 10.1021/acsami.5b01658
ACS Appl. Mater. Interfaces 2015, 7, 13342−13349

The absorption profiles of glass/ITO/PEDOT:PSS/P3HT:PCBM films without further treatment (untreated) and those treated with Pre-TA, CVSVA, or HPSVA are shown in Figure 4a. The peak intensities of treated films are

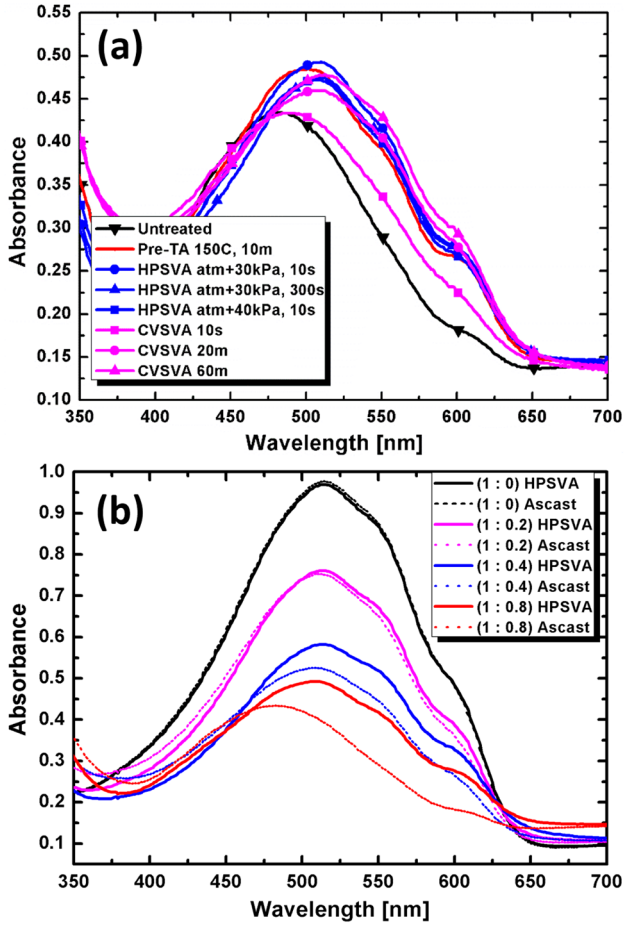


**Figure 4.** (a) Light absorption profiles of untreated, prethermally annealed (Pre-TA) at 150 °C for 10 min, conventional solvent vapor annealed (CVSVA), and high-pressure solvent vapor annealed (HPSVA) films with vapor pressure and execution time. (b) Light absorption profiles according to P3HT:PCBM ratio.

higher compared to untreated films, regardless of the annealing method. Moreover, the $\pi-\pi$ stacking structure of P3HT lamellae are indicated by the absorbance peaks[38] at 550 and 603 nm in both the thermally annealed and HPSVA films. However, a significant difference in peak intensities is not observed; we speculate that the amount of exciton generation from light absorption is similar for both thermally annealed and HPSVA-treated films. Interestingly, a red-shift at the maximum absorption appears in the HPSVA films. A red-shift in the optical absorption is observed when the effective conjugation length of the P3HT chain segments is increased in densely packed crystallites.[6,20,33] This increases the number of delocalized electrons, narrows the band gap, and consequently facilitates electron excitation at weaker light energies near the infrared region. During HPSVA, high-pressure acetone molecules compress the active layer and form closely packed P3HT crystallites. Compared to the film annealed at 30 kPa for 10 s, a slight absorbance reduction is observed in the film processed under higher pressure (40 kPa, 10 s) or for a longer exposure time (30 kPa, 300 s). This slight reduction might come from the decreased thickness of the active layer caused by excessive HPSVA, which is shown in the TOF-SIMS profile in Figure 2. CVSVA film treated for 10 s shows a similar absorption profile as the untreated film, and a crystallization peak at 550 and 603 nm does not appear. Over 20 min of treatment, it eventually has a similar profile to the HPSVA film. This means that P3HT crystallization under CVSVA treatment takes time because of low pressure. Absorbance profiles of various P3HT:PCBM ratios are shown in Figure 4b. Here, HPSVA was conducted at 30 kPa of pressure for 10 s. As the PCBM concentration increases, absorbance of P3HT:PCBM decreases. It is known that the P3HT crystallization is hindered by the presence of PCBM,[39] so pure P3HT film without PCBM (ratio 1:0) shows very high absorbance even before HPSVA. In the pure P3HT film, HPSVA treatment does not increase the crystallinity because it is already sufficiently crystallized. The HPSVA treatment increases the P3HT crystallinity when the P3HT:PCBM ratio is more than 0.4, and the effect of treatment become more successful when the ratio increases as shown in Figure 4b. This indicates that the HPSVA indeed influences the crystallinity of the P3HT.

The lateral phase distribution of P3HT and PCBM was investigated through the use of tapping mode atomic force microscopy (AFM), in which a cantilever beam equipped with AFM scans the surface of the active layer, and the vibration of the beam changes depending on whether the phase is soft or hard.[40,41] P3HT- and PCBM-rich domains are relatively softer and harder, so their phases appeared as brighter and darker regions in the AFM phase images, respectively.[42] Supporting Information presents AFM phase images obtained for films that were (a) untreated, (b) Pre-TA at 150 °C for 10 min, (c) HPSVA at 30 kPa for 10 s, and (d) HPSVA at 40 kPa for 10 s. In Figure S1b, Supporting Information, bright, long nanofibers, which are P3HT lamellae formed during Pre-TA, are clearly observed. This result is consistent with the aforementioned XRD profile. The HPSVA films in Figure S1c,d, Supporting Information, show bright regions that are slightly larger than those in the untreated film, but they do not show any long nanofibers. This means that P3HT does not become fully crystallized during HPSVA because acetone is a nonsolvent for P3HT. The phase images of the HPSVA films show larger dark regions compared to those of the untreated and thermally annealed films; dark regions as large as 100 nm are observed in the film annealed by HPSVA at 40 kPa for 10 s.

This could imply that PCBM molecules aggregate or migrate to the top surface of the active layer during HPSVA. Although the vertical migration cannot be predicated, it is certain that it contributed to making the dark region on the top surface. This result is consistent with the lower sulfur to carbon ratio shown in the TOF-SIMS profile. A greater concentration of the PCBM-rich phase near the top surface is beneficial to free charge carrier transport; however, excessively large phases hinder exciton dissociation due to the lower interfacial area between the electron and donor materials.[43]

The performance of a representative HPSVA film annealed at 30 kPa for 10 s is shown in Figure 5. The detailed results of all of the various annealing conditions are shown in Table 2. Thermally annealed and HPSVA (30 kPa, 10 s) films show similar PCEs, but the HPSVA film exhibits a higher short circuit current density ($J_{sc}$) of 5.6 mA/cm$^2$ compared to the thermally annealed film (5.04 mA/cm$^2$). The $J_{sc}$ is related to the degree of light absorption, exciton dissociation rate, and charge transport rate. Both HPSVA and thermally annealed films show similar


DOI: 10.1021/acsami.5b01658
ACS Appl. Mater. Interfaces 2015, 7, 13342−13349

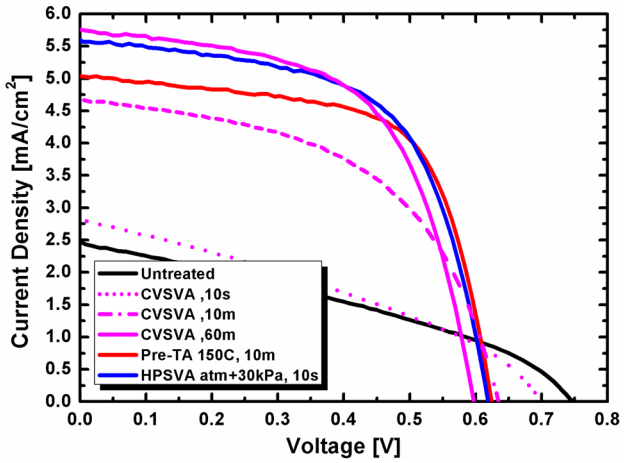


**Figure 5.** Current density and voltage curves of untreated, thermally annealed (Pre-TA) at 150 °C for 10 min, conventional solvent vapor annealed (CVSVA), and high-pressure solvent vapor annealed (HPSVA) films at 30 kPa for 10 s.

light absorbance profiles in Figure 4; the amount of exciton generation is also expected to be similar. In these analogous conditions, the enhancement of $J_{sc}$ could be explained by an improved exciton dissociation rate and by improvement in free charge carrier transport. During HPSVA, a large interfacial area is formed between P3HT and PCBM; this phenomenon is inferred from the small phase separation observed in the AFM phase images and from the weak crystallization peak in the XRD profile. This large interfacial area facilitates the dissociation of Frenkel excitons, which have short exciton diffusion lengths (~10 nm).[43−45] Once the free charge carriers are generated via exciton dissociation, they can be extracted to their corresponding electrodes. If hole-conducting materials are dominant near the cathode (the distribution that typically appears in thermally annealed films), free electrons drifting toward the upper cathode might be attracted to free holes in the P3HT; these charges could be dissipated via bimolecular recombination.[4,5] However, HPSVA films exhibit a PCBM-rich phase near the top surface (as shown in the TOF-SIMS profiles), indicating that free electrons can be effectively transferred to the cathode.

The open circuit voltage ($V_{oc}$) in the HPSVA films was reduced to around 0.6 eV (from 0.75 eV in the untreated film). Lyons et al. obtained a similar $V_{oc}$ reduction to 0.58−0.64 eV (from 0.7 eV) when their films were treated with SVA or Pre-TA; this reduction was attributed to a reduction in the band gap.[46] They stated that more delocalized electrons are generated by the higher crystallinity of P3HT and larger PCBM clusters. These electrons reduce the energy difference between the highest occupied molecular orbital (HOMO) of P3HT and the lowest unoccupied molecular orbital (LUMO) of PCBM. In our experiment, the XRD profile and absorption peak intensities showed an increase in the number of local P3HT crystallites in the HPSVA films. We suspect that the reason that the pressurized solvent plays a benign role in improving the morphology is that acetone molecules smear into empty spaces in the P3HT and PCBM mixture owing to their small size. Then, the energy of the acetone molecules is dissipated into the layers of the P3HT and PCBM mixture, which enables morphological evolution.

The CVSVA film treated around 30 min showed the analogous PCE with HPSVA films, but the resulting morphologies were analogous. The absorbance, XRD, and SIMS profiles of CVSVA were analogous to those of HPSVA. HPSVA reduced the treatment time owing to high pressure. Unlike CVSVA, where diffusion transport is dominated, both the advection and diffusion of acetone molecules occur in HPSVA, which make morphology evolution rapid.

To examine the applicability of HPSVA in the roll-to-roll process, we conducted similar experiments to those described above, but the high-pressure solvent vapor was injected into a sample under atmospheric pressure, HPSVA (atm). Continuously maintaining high-pressure conditions via a sealed environment would be difficult during mass production because films move along a roll-to-roll fabrication system. Therefore, in this experiment, the substrate was placed in ambient conditions. High-pressure solvent vapor was similarly generated using an intercept valve. When the solvent vapor was vented through the intercept valve, the film substrate was exposed to high-pressure

**Table 2. Power Conversion Efficiency (PCE), Short Circuit Current Density ($J_{sc}$), Open Circuit Voltage ($V_{oc}$), and Fill Factor (FF)[a]**

| | PCE [%] | $J_{sc}$ [mA/cm$^2$] | $V_{oc}$ [V] | FF | PCE_avg ($\sigma$) [%] |
|---|---|---|---|---|---|
| untreated | 0.64 | 2.48 | 0.75 | 0.35 | 0.62 (0.025) |
| pre-TA (150 °C, 10 m) | 2.04 | 5.04 | 0.62 | 0.65 | 1.95 (0.086) |
| HPSVA (atm + 10 kPa, 10 s) | 1.95 | 5.32 | 0.62 | 0.59 | 1.82 (0.090) |
| HPSVA (atm + 20 kPa, 10 s) | 2.07 | 5.59 | 0.62 | 0.60 | 1.94 (0.128) |
| HPSVA (atm + 30 kPa, 5 s) | 2.05 | 5.60 | 0.61 | 0.60 | 1.97 (0.057) |
| HPSVA (atm + 30 kPa, 10 s) | 2.09 | 5.60 | 0.62 | 0.60 | 1.97 (0.074) |
| HPSVA (atm + 30 kPa, 60 s) | 2.01 | 5.75 | 0.60 | 0.58 | 1.82 (0.322) |
| HPSVA (atm + 30 kPa, 300 s) | 1.84 | 5.52 | 0.60 | 0.56 | 1.74 (0.123) |
| HPSVA (atm + 40 kPa, 10 s) | 1.97 | 5.44 | 0.61 | 0.60 | 1.87 (0.072) |
| HPSVA (atm, 10 s) | 1.78 | 5.41 | 0.61 | 0.54 | 1.57 (0.214) |
| CVSVA (10 s) | 0.68 | 2.84 | 0.70 | 0.34 | 0.65 (0.022) |
| CVSVA (10 m) | 1.55 | 4.67 | 0.63 | 0.52 | 1.49 (0.037) |
| CVSVA (30 m) | 1.97 | 5.54 | 0.61 | 0.58 | 1.87 (0.059) |
| CVSVA (60 m) | 2.02 | 5.76 | 0.60 | 0.59 | 1.99 (0.019) |

[a]Presented according to the treatment conditions: untreated, pre-thermally annealed (Pre-TA) at 150°C for 10 min, conventional solvent vapor annealed (CVSVA), and high-pressure solvent vapor annealed (HPSVA) at various pressures and exposure times. atm, atmospheric pressure. Here, PCE_avg is the average value of PCEs, and $\sigma$ is standard deviation of PCEs.


DOI: 10.1021/acsami.5b01658
ACS Appl. Mater. Interfaces 2015, 7, 13342−13349

solvent vapor. The pressure was 30 kPa before opening the intercept valve, and the exposure time was 10 s. Films processed in this manner also showed enhanced PCE over that of untreated films, as indicated in Table 2. The temperature during HPSVA was around 56 °C, which is the boiling point of acetone. Also, the film temperature was measured to be around 56 °C with an infrared thermometer. This indicates that the film, which was initially at room temperature, quickly thermalizes to that of the vapor. We found that condensation occurred initially, but it was quickly vaporized due to the volatility in addition to the high convection of the pressurized vapor. Therefore, once the substrate reached the steady state temperature, the effect of condensation could be negligible. Although the PCE of films treated via this method was not as high as those treated via Pre-TA or the rigorously sealed HPSVA films, optimizing exposure time and injection pressure conditions should resolve this issue. Additionally, acetone is relatively less toxic than many other solvents, such as chlorobenzene, dichlorobenzene, or 2-chlorophenol; its use could help facilitate mass production. Therefore, we expect that the HPSVA method could be adapted to a roll-to-roll system. For mass fabrication, the rolling film substrate can be directly exposed to high-pressure acetone vapor by placing the vapor vent nozzle very close to the active layer under ambient conditions.

## 3. CONCLUSION

A HPSVA method employing a benign solvent (acetone) was used to achieve rapid solvent vapor annealing. HPSVA films treated at 30 kPa for 10 s showed optimum performance. Acetone is a nonsolvent for P3HT but can dissolve small amounts of PCBM. Acetone vapor molecules can penetrate into the active layer under high vapor pressure conditions and alter the morphology. HPSVA induces a PCBM-rich phase near the cathode and facilitates the transport of free charge carriers to the electrode. Although P3HT is not soluble in acetone, temporary vacancies can be generated during the process of PCBM diffusion, allowing P3HT lamellae to be locally rearranged. The high-pressure acetone molecules formed during HPSVA compressed the active layer and formed close-packed P3HT crystallites, leading to OPV films with enhanced performance. The enhanced PCE originates from the interplay between increased $J_{sc}$ and decreased FF. The HPSVA films show small phase separation and a PCBM-rich phase near the cathode which decreases and increases the FF, respectively. This mutual influence shows a FF of 0.6 of the HPSVA film which is lower than that of the pre-TA film (0.65). However, from the point of view of exciton dissociation, small phase separation is beneficial for charge generation which will induce high $J_{sc}$. The HPSVA film shows a $J_{sc}$ of 5.60 mA/cm$^2$ which is higher than that of the pre-TA film (5.04 mA/cm$^2$). In summary, HPSVA treatment generates small phase separation while making a PCBM-rich phase near the cathode, which induces enhanced $J_{sc}$ and moderate FF, which finally leads to increased PCE.

The HPSVA treatment using acetone may influence the PEDOT:PSS layer if acetone solvent penetrated and reached to the PEDOT:PSS layer, which could reduce the resistivity of the PEDOT:PSS layer, which could be beneficial to the device performance.[47] Irrespective of this, XRD, absorbance data, AFM, and SIMS profiles implied that the active layer morphology evolution exists. However, we assigned effects of HPSVA on the PEDOT:PSS layer as a future study since the main point of this paper is morphology evolution of the active layer.

## 4. EXPERIMENTAL SECTION

**Device Fabrication.** Poly(3-hexylthiophene-2,5-diyl) (P3HT, molecular weight ~50 000 g mol$^{-1}$, 90–94% regioregular, Rieke Metals) and 1-(3-methoxycarbonyl)-propyl-1,1-phenyl-(6,6)C61 (PCBM, Nano-C) were dissolved in chlorobenzene at 20 and 16 mg mL$^{-1}$, respectively, stirred overnight, and then blended together for more than 12 h. Patterned indium tin oxide (ITO, sheet resistance 10Ω/□) on a glass substrate was rinsed with detergent, deionized water, acetone, and isopropyl alcohol by sonication and then dried with $N_2$ gas. The substrates were treated with a UV ozone cleaner for 10 min and then transferred into a glovebox filled with $N_2$ gas (moisture <0.1 ppm and oxygen <1 ppm). The 40 nm layers of poly(3,4-ethylenedioxythiophene):poly(styrenesulfonate) (PEDOT:PSS, Clevios P VP AL 4083) were spin-coated (2500 rpm, 60 s) on the ITO glass and cured on a hot plate (140 °C, 10 min). The active layer (100 nm in thickness) of P3HT:PCBM was spin-coated on the PEDOT:PSS film and then either thermally annealed (150 °C, 10 min) or high-pressure solvent vapor annealed. To ensure a fair comparison, all of the samples were exposed to air for about 1 h during HPSVA. LiF (0.5 nm in thickness) and an aluminum cathode (100 nm in thickness) were consecutively deposited in a thermal evaporator at 2 × 10$^{-6}$ Torr. High-pressure acetone vapor was generated by heating acetone in a sealed 1 L flask. Acetone solvent vapor molecules were evaporated in the flask after it was wrapped with a heating mantle (Wise Therm WHM). Above the acetone boiling point (56 °C), the pressure in the large flask increased. After reaching the target pressure, the intercept valve was opened and the high-pressure solvent vapor was transferred into a connected 50 mL flask. The pressure was also measured with a pressure gauge attached to the small flask, and the pressure difference caused by opening the valve was less than 10%. A film in the small flask was annealed with the high-pressure solvent vapor for a specific exposure time from 5 to 300 s. The "atm" HPSVA film was exposed to prepressured acetone vapor (30 kpa in a large flask) at atmospheric pressure for 10 s.

**Characterization.** Current–voltage characterization was performed under an AM1.5G filtered light (100 mW cm$^{-2}$) solar simulator (SAN-EI, XES-301S) using a Keithley 2400 source meter. The absorbance of the samples was measured with a UV/vis/NIR spectrometer (PerkinElmer, Lambda 750). XRD profiles were obtained with an Ultima IV (Rigaku) using a Cu K$\alpha_1$ source with an X-ray generation power of 3 kW. The diffraction spectra were measured in the $\theta$–$2\theta$ symmetry mode. AFM phase image measurements were conducted in tapping mode with a Nanowizard I (JPK inst.). A silicon cantilever (APPNANO-ACTA20; aluminum-coated; force constant: 37 N m$^{-1}$; resonance frequency: 300 kHz) with a silicon tip (pyramidal shape, tip radius <10 nm) was used for phase imaging. TOF-SIMS profiles were evaluated using an ION-TOF (Münster, Germany) equipped with a sputter gun ($Cs^+$, 3 keV, 32 nA, 300 $\mu$m × 300 $\mu$m) and an analysis gun ($Bi^{3+}$, 25 keV, 0.2 pA, 100 × 100 $\mu$m$^2$). The solubilities of P3HT and PCBM in acetone were measured via UV–vis spectroscopy (SINCO 4100) and calculated using the Beer–Lambert Law. Excess amounts of P3HT and PCBM were dissolved in acetone and stirred for 2 weeks. Then, any undissolved materials were precipitated via centrifugation (Fisher Scientific 228) at 3000 rpm for 10 min. After centrifugation, the absorbance of the remaining acetone, which contained the maximum concentration of solute, was measured via UV–vis spectroscopy.

## ■ ASSOCIATED CONTENT

### Supporting Information

AFM phase contrast images of top surface according to annealing methods are provided in the Supporting Information. The Supporting Information is available free of charge on the ACS Publications website at DOI: 10.1021/acsami.5b01658.



DOI: 10.1021/acsami.5b01658
ACS Appl. Mater. Interfaces 2015, 7, 13342–13349

## AUTHOR INFORMATION


### Corresponding Author

*E-mail: woochul@yonsei.ac.kr.


### Notes

The authors declare no competing financial interest.

## ACKNOWLEDGMENTS

This work was supported by the National Research Foundation of Korea (NRF) Grant (No. 2011-0028729) funded by the Korean Government Ministry of Education, Science and Technology (MEST) and Business for Cooperative R&D between Industry, Academy, and Research Institute (Grant No. C0186875) funded Korea Small and Medium Business Administration in 2014. This work was supported in part by the Yonsei University Research Fund of 2014.

## REFERENCES


(1) Peet, J.; Kim, J. Y.; Coates, N. E.; Ma, W. L.; Moses, D.; Heeger, A. J.; Bazan, G. C. Efficiency Enhancement in Low-Bandgap Polymer Solar Cells by Processing with Alkane Dithiols. *Nat. Mater.* **2007**, *6*, 497−500.

(2) Yao, Y.; Hou, J.; Xu, Z.; Li, G.; Yang, Y. Effects of Solvent Mixtures on the Nanoscale Phase Separation in Polymer Solar Cells. *Adv. Funct. Mater.* **2008**, *18*, 1783−1789.

(3) He, X.; Gao, F.; Tu, G.; Hasko, D.; Hüttner, S.; Steiner, U.; Greenham, N. C.; Friend, R. H.; Huck, W. T. S. Formation of Nanopatterned Polymer Blends in Photovoltaic Devices. *Nano Lett.* **2010**, *10*, 1302−1307.

(4) He, X.; Gao, F.; Tu, G.; Hasko, D. G.; Hüttner, S.; Greenham, N. C.; Steiner, U.; Friend, R. H.; Huck, W. T. S. Formation of Well-Ordered Heterojunctions in Polymer:PCBM Photovoltaic Devices. *Adv. Funct. Mater.* **2011**, *21*, 139−146.

(5) Chen, D.; Zhao, W.; Russell, T. P. P3HT Nanopillars for Organic Photovoltaic Devices Nanoimprinted by AAO Templates. *ACS Nano* **2012**, *6*, 1479−1485.

(6) Li, G.; Shrotriya, V.; Huang, J. S.; Yao, Y.; Moriarty, T.; Emery, K.; Yang, Y. High-Efficiency Solution Processable Polymer Photovoltaic Cells by Self-Organization of Polymer Blends. *Nat. Mater.* **2005**, *4*, 864−868.

(7) van Bavel, S. S.; Sourty, E.; de With, G.; Loos, J. Three-Dimensional Nanoscale Organization of Bulk Heterojunction Polymer Solar Cells. *Nano Lett.* **2009**, *9*, 507−513.

(8) Watts, B.; Belcher, W. J.; Thomsen, L.; Ade, H.; Dastoor, P. C. A Quantitative Study of PCBM Diffusion during Annealing of P3HT:PCBM Blend Films. *Macromolecules* **2009**, *42*, 8392−8397.

(9) Yu, B. Y.; Lin, W. C.; Wang, W. B.; Iida, S.; Chen, S. Z.; Liu, C. Y.; Kuo, C. H.; Lee, S. H.; Kao, W. L.; Yen, G. J.; You, Y. W.; Liu, C. P.; Jou, J. H.; Shyue, J. J. Effect of Fabrication Parameters on Three-Dimensional Nanostructures of Bulk Heterojunctions Imaged by High-Resolution Scanning ToF-SIMS. *ACS Nano* **2010**, *4*, 833−840.

(10) Wu, J. L.; Chen, F. C.; Hsiao, Y. S.; Chien, F. C.; Chen, P. L.; Kuo, C. H.; Huang, M. H.; Hsu, C. S. Surface Plasmonic Effects of Metallic Nanoparticles on the Performance of Polymer Bulk Heterojunction Solar Cells. *ACS Nano* **2011**, *5*, 959−967.

(11) Li, G.; Yao, Y.; Yang, H.; Shrotriya, V.; Yang, G.; Yang, Y. "Solvent Annealing" Effect in Polymer Solar Cells Based on Poly(3-hexylthiophene) and Methanofullerenes. *Adv. Funct. Mater.* **2007**, *17*, 1636−1644.

(12) Campoy-Quiles, M.; Ferenczi, T.; Agostinelli, T.; Etchegoin, P. G.; Kim, Y.; Anthopoulos, T. D.; Stavrinou, P. N.; Bradley, D. D. C.; Nelson, J. Morphology Evolution via Self-Organization and Lateral and Vertical Diffusion in Polymer:Fullerene Solar Cell Blends. *Nat. Mater.* **2008**, *7*, 158−164.

(13) Miller, S.; Fanchini, G.; Lin, Y. Y.; Li, C.; Chen, C. W.; Su, W. F.; Chhowalla, M. Investigation of Nanoscale Morphological Changes in Organic Photovoltaics During Solvent Vapor Annealing. *J. Mater. Chem.* **2008**, *18*, 306−312.

(14) Park, J. H.; Kim, J. S.; Lee, J. H.; Lee, W. H.; Cho, K. Effect of Annealing Solvent Solubility on the Performance of Poly(3-hexylthiophene)/Methanofullerene Solar Cells. *J. Phys. Chem. C* **2009**, *113*, 17579−17584.

(15) Ko, C. J.; Lin, Y. K.; Chen, F. C. Microwave Annealing of Polymer Photovoltaic Devices. *Adv. Mater.* **2007**, *19*, 3520−3523.

(16) Yoshikawa, O.; Sonobe, T.; Sagawa, T.; Yoshikawa, S. Single Mode Microwave Irradiation to Improve the Efficiency of Polymer Solar Cell Based on Poly(3-hexylthiophene) and Fullerene Derivative. *Appl. Phys. Lett.* **2009**, *94*, 083301.

(17) Flugge, H.; Schmidt, H.; Riedl, T.; Schmale, S.; Rabe, T.; Fahlbusch, J.; Danilov, M.; Spieker, H.; Schobel, J.; Kowalsky, W. Microwave Annealing of Polymer Solar Cells with Various Transparent Anode Materials. *Appl. Phys. Lett.* **2010**, *97*, 123306.

(18) Li, H.; Tang, H.; Li, L.; Xu, W.; Zhao, X.; Yang, X. Solvent-Soaking Treatment Induced Morphology Evolution in P3HT/PCBM Composite Films. *J. Mater. Chem.* **2011**, *21*, 6563−6568.

(19) Han, B.; Gopalan, S.-A.; Lee, K.-D.; Kang, B.-H.; Lee, S.-W.; Lee, J.-S.; Kwon, D.-H.; Lee, S.-H.; Kang, S.-W. Preheated Solvent Exposure on P3HT:PCBM Thin Film: A Facile Strategy to Enhance Performance in Bulk Heterojunction Photovoltaic Cells. *Curr. Appl. Phys.* **2014**, *14*, 1443−1450.

(20) Yu-Xuan, L.; L.-F, L.; Yu, N.; Yun-Zhang, L.; Qi-Peng, L.; Chun-Mei, Z.; Yi, F.; Ai-Wei, T.; Yu-Feng, H.; Zhi-Dong, L.; Feng, T.; Yan-Bing, H. Effects of Acetone-Soaking Treatment on the Performance of Polymer Solar Cells Based on P3HT/PCBM Bulk Heterojunction. *Chin. Phys. B* **2014**, *23*, 118802.

(21) Lim, B.; Jo, J.; Na, S.-I.; Kim, J.; Kim, S.-S.; Kim, D.-Y. A Morphology Controller for High-Efficiency Bulk-Heterojunction Polymer Solar Cells. *J. Mater. Chem.* **2010**, *20*, 10919−10923.

(22) Chu, T. Y.; Lu, J. P.; Beaupre, S.; Zhang, Y. G.; Pouliot, J. R.; Wakim, S.; Zhou, J. Y.; Leclerc, M.; Li, Z.; Ding, J. F.; Tao, Y. Bulk Heterojunction Solar Cells Using Thieno[3,4-c]pyrrole-4,6-dione and Dithieno[3,2-b:2′,3′-d]silole Copolymer with a Power Conversion Efficiency of 7.3%. *J. Am. Chem. Soc.* **2011**, *133*, 4250−4253.

(23) Su, M. S.; Kuo, C. Y.; Yuan, M. C.; Jeng, U. S.; Su, C. J.; Wei, K. H. Improving Device Efficiency of Polymer/Fullerene Bulk Heterojunction Solar Cells Through Enhanced Crystallinity and Reduced Grain Boundaries Induced by Solvent Additives. *Adv. Mater.* **2011**, *23*, 3315−3319.

(24) Huang, Y. C.; Welch, G. C.; Bazan, G. C.; Chabinyc, M. L.; Su, W. F. Self-Vertical Phase Separation Study of Nanoparticle/Polymer Solar Cells by Introducing Fluorinated Small Molecules. *Chem. Commun.* **2012**, *48*, 7250−7252.

(25) Liu, F.; Zhao, W.; Tumbleston, J. R.; Wang, C.; Gu, Y.; Wang, D.; Briseno, A. L.; Ade, H.; Russell, T. P. Understanding the Morphology of PTB7:PCBM Blends in Organic Photovoltaics. *Adv. Energy Mater.* **2014**, *4*, 1301377.

(26) Kim, M.; Kim, J.-H.; Choi, H. H.; Park, J. H.; Jo, S. B.; Sim, M.; Kim, J. S.; Jinnai, H.; Park, Y. D.; Cho, K. Electrical Performance of Organic Solar Cells with Additive-Assisted Vertical Phase Separation in the Photoactive Layer. *Adv. Energy Mater.* **2014**, *4*, 1300612.

(27) Ruderer, M. A.; Guo, S.; Meier, R.; Chiang, H. Y.; Korstgens, V.; Wiedersich, J.; Perlich, J.; Roth, S. V.; Muller-Buschbaum, P. Solvent-Induced Morphology in Polymer-Based Systems for Organic Photovoltaics. *Adv. Funct. Mater.* **2011**, *21*, 3382−3391.

(28) Guo, S.; Herzig, E. M.; Naumann, A.; Tainter, G.; Perlich, J.; Muller-Buschbaum, P. Influence of Solvent and Solvent Additive on the Morphology of PTB7 Films Probed via X-ray Scattering. *J. Phys. Chem. B* **2014**, *118*, 344−350.

(29) Meier, R.; Schindler, M.; Muller-Buschbaum, P.; Watts, B. Residual Solvent Content in Conducting Polymer-Blend Films Mapped with Scanning Transmission X-ray Microscopy. *Phys. Rev. B* **2011**, *84*, 174205.

(30) Jo, J.; Na, S. I.; Kim, S. S.; Lee, T. W.; Chung, Y.; Kang, S. J.; Vak, D.; Kim, D. Y. Three-Dimensional Bulk Heterojunction Morphology for Achieving High Internal Quantum Efficiency in Polymer Solar Cells. *Adv. Funct. Mater.* **2009**, *19*, 2398−2406.




DOI: 10.1021/acsami.5b01658
*ACS Appl. Mater. Interfaces* 2015, 7, 13342−13349

(31) Burgues-Ceballos, I.; Campoy-Quiles, M.; Francesch, L.; Lacharmoise, P. D. Fast Annealing and Patterning of Polymer Solar Cells by Means of Vapor Printing. *J. Polym. Sci., Part B: Polym. Phys.* **2012**, *50*, 1245−1252.
(32) Hu, S.; Dyck, O.; Chen, H. P.; Hsiao, Y. C.; Hu, B.; Duscher, G.; Dadmun, M.; Khomami, B. The Impact of Selective Solvents on the Evolution of Structure and Function in Solvent Annealed Organic Photovoltaics. *RSC Adv.* **2014**, *4*, 27931−27938.
(33) Tang, H.; Lu, G.; Li, L.; Li, J.; Wang, Y.; Yang, X. Precise Construction of PCBM Aggregates for Polymer Solar Cells via Multi-Step Controlled Solvent Vapor Annealing. *J. Mater. Chem.* **2010**, *20*, 683−688.
(34) Sirringhaus, H.; Brown, P. J.; Friend, R. H.; Nielsen, M. M.; Bechgaard, K.; Langeveld-Voss, B. M. W.; Spiering, A. J. H.; Janssen, R. A. J.; Meijer, E. W.; Herwig, P.; De Leeuw, D. M. Two-Dimensional Charge Transport in Self-Organized, High-Mobility Conjugated Polymers. *Nature* **1999**, *401*, 685−688.
(35) Brinkmann, M.; Contal, C.; Kayunkid, N.; Djuric, T.; Resel, R. Highly Oriented and Nanotextured Films of Regioregular Poly(3-hexylthiophene) Grown by Epitaxy on the Nanostructured Surface of an Aromatic Substrate. *Macromolecules* **2010**, *43*, 7604−7610.
(36) Salammal Shabi, T.; Grigorian, S.; Brinkmann, M.; Pietsch, U.; Koenen, N.; Kayunkid, N.; Scherf, U. Enhancement in Crystallinity of Poly(3-hexylthiophene) Thin Films Prepared by Low-Temperature Drop Casting. *J. Appl. Polym. Sci.* **2012**, *125*, 2335−2341.
(37) Verploegen, E.; Miller, C. E.; Schmidt, K.; Bao, Z. N.; Toney, M. F. Manipulating the Morphology of P3HT-PCBM Bulk Heterojunction Blends with Solvent Vapor Annealing. *Chem. Mater.* **2012**, *24*, 3923−3931.
(38) Kekuda, D.; Lin, H.-S.; Wu, M. C.; Huang, J.-S.; Ho, K.-C.; Chu, C.-W. The Effect of Solvent Induced Crystallinity of Polymer Layer on Poly(3-hexylthiophene)/C70 Bilayer Solar Cells. *Sol. Energy Mater. Sol. Cells* **2011**, *95*, 419−422.
(39) Kohn, P.; Rong, Z. X.; Scherer, K. H.; Sepe, A.; Sommer, M.; Muller-Buschbaum, P.; Friend, R. H.; Steiner, U.; Huttner, S. Crystallization-Induced 10-nm Structure Formation in P3HT/PCBM Blends. *Macromolecules* **2013**, *46*, 4002−4013.
(40) Cleveland, J. P.; Anczykowski, B.; Schmid, A. E.; Elings, V. B. Energy Dissipation in Tapping-Mode Atomic Force Microscopy. *Appl. Phys. Lett.* **1998**, *72*, 2613−2615.
(41) Dutta, P.; Xie, Y.; Kumar, M.; Rathi, M.; Ahrenkiel, P.; Galipeau, D.; Qiao, Q. Q.; Bommisetty, V. Connecting Physical Properties of Spin-Casting Solvents with Morphology, Nanoscale Charge Transport, and Device Performance of Poly(3-hexylthiophene):Phenyl-C-61-butyric Acid Methyl Ester Bulk Heterojunction Solar Cells. *J. Photonics Energy* **2011**, *1*, 11124.
(42) Thormann, E.; Pettersson, T.; Kettle, J.; Claesson, P. M. Probing Material Properties of Polymeric Surface Layers with Tapping Mode AFM: Which Cantilever Spring Constant, Tapping Amplitude and Amplitude Set Point Gives Good Image Contrast and Minimal Surface Damage? *Ultramicroscopy* **2010**, *110*, 313−319.
(43) Yang, X.; Loos, J. Toward High-Performance Polymer Solar Cells: The Importance of Morphology Control. *Macromolecules* **2007**, *40*, 1353−1362.
(44) Halls, J. J. M.; Pichler, K.; Friend, R. H.; Moratti, S. C.; Holmes, A. B. Exciton Diffusion and Dissociation in a Poly(*p*-phenylenevinylene)/C60 Heterojunction Photovoltaic Cell. *Appl. Phys. Lett.* **1996**, *68*, 3120−3122.
(45) Haugeneder, A.; Neges, M.; Kallinger, C.; Spirkl, W.; Lemmer, U.; Feldmann, J.; Scherf, U.; Harth, E.; Gügel, A.; Müllen, K. Exciton Diffusion and Dissociation in Conjugated Polymer/Fullerene Blends and Heterostructures. *Phys. Rev. B* **1999**, *59*, 15346−15351.
(46) Lyons, B. P.; Clarke, N.; Groves, C. The Relative Importance of Domain Size, Domain Purity and Domain Interfaces to the Performance of Bulk-Heterojunction Organic Photovoltaics. *Energy Environ. Sci.* **2012**, *5*, 7657−7663.
(47) Yang, J. S.; Oh, S. H.; Kim, D. L.; Kim, S. J.; Kim, H. J. Hole Transport Enhancing Effects of Polar Solvents on Poly(3,4-ethylenedioxythiophene):Poly(styrene sulfonic acid) for Organic Solar Cells. *ACS Appl. Mater. Interfaces* **2012**, *4*, 5394−5398.


DOI: 10.1021/acsami.5b01658
*ACS Appl. Mater. Interfaces* 2015, 7, 13342−13349